

TOWARDS UNDERSTANDING THE FORMATION AND STABILITY OF NANOMETER SCALE Y-Ti-O CLUSTERS IN NANOSTRUCTURED FERRITIC ALLOYS USING LATTICE-BASED MONTE CARLO SIMULATIONS—M. J. Alinger and B. D. Wirth (University of California, Berkeley)

OBJECTIVE

The objective of this study is to explore the factors that control the formation, stability and composition of Y-Ti-O nanoclusters (NCs) in nanostructured ferritic alloys (NFAs) using Lattice-based Monte Carlo (LMC) simulations.

SUMMARY

Lattice-based Monte Carlo (LMC) simulations are currently being developed to better understand the formation and stability of nm-scale clusters, or nanoclusters (NCs), in nanostructured ferritic alloys (NFAs). NFAs typically have a nominal composition in the range of Fe-(13-15) at %Cr-(0-1)W-(0.25-1)Ti-(0.1-0.25)Y-(0.15-0.40)O. A key fundamental issue is the local atomic arrangement (structure) and chemistry of the Y-Ti-O NCs. The LMC program has been written, debugged and the alloy thermodynamics have been verified against phase diagrams over the past several months. Bond energies have been obtained from calculations of the mixing enthalpies within a regular-solution thermodynamics model, making the simplification of a pure Fe (as opposed to Fe-14Cr) matrix and omitting the impurity elements. The mixing enthalpies have been obtained from the free energies for Y, Ti and O solute atoms. The simulations are performed on a body-centered cubic lattice, with oxygen situated on an octahedral interstitial sub-lattice. NC evolution is being simulated starting from a random super-saturated solution. The resulting structures will be compared to experimental observations by transmission electron microscopy, small angle neutron scattering, atom probe tomography and positron annihilation spectroscopy. Combined, these results will provide atomic-level insight into the NC structure and chemistry and provide a basis for optimizing NFA development as well as understanding the thermal and radiation stability of the NCs.

PROGRESS AND STATUS

Introduction

Nanostructured ferritic alloys (NFAs) are promising candidates for high temperature structural materials, tailored specifically for fusion environments [1,2]. The key component in these alloys is a high density ($>10^{22} \text{ m}^{-3}$) of nm-scale ($r = 1-2 \text{ nm}$) clusters or precipitates which can act to impede dislocation motion at elevated temperatures as well as provide sink sites for radiation damage and transmutation He. Studies using small angle neutron scattering (SANS) and atom probe tomography (APT) have shown that certain combinations of alloy chemistry and processing are capable of forming such nanoclusters [1,3,4]. These studies have revealed the key components for NC formation as well as the effective precipitation energy and thermal stability. However, many details are still elusive and computational simulations can provide valuable insight on the atomic scale.

Monte Carlo Model and Simulation Technique

Atomistic Model

A lattice-based Monte Carlo (LMC) model has been developed to simulate the atomic scale configuration of Y-Ti-O nanoclusters in nanostructured ferritic alloys (NFAs). Several simplifying assumptions are made regarding the alloy composition. First, the chromium, which does not play an obvious role in the formation of NCs, is omitted from the simulations. Second, the tungsten, which has been shown not to play a role in NC formation [4], is also not included. Therefore, the alloy chemistry simulated is Fe-0.47at%Ti-0.12Y-0.19O, as opposed to Fe-15at%Cr-0.91W-0.47Ti-0.12Y-0.19O. As oxygen typically resides in octahedral

interstitial lattice sites in iron, the simulation employs two sub-lattices (BCC and octahedral interstitial) to accurately describe the system.

The simulation cell, with periodic boundary conditions, contains a specified number of solute atoms on rigid lattice sites, with the initial condition of a random solid solution. The simulation evaluates the exchanges of the solute atoms with their i ($i = 1-8$ for BCC and $i = 1-12$ for Octahedral) first nearest neighbors (1NN) based on the Boltzmann weighted probabilities, P_i , defined as:

$$P_i = \exp\left(\frac{-\Delta E}{kT}\right) \text{ for } \Delta E \geq 0 \text{ or } 1 \text{ for } \Delta E < 0 \quad (1)$$

Where E is the total system energy at a state and ΔE is the change in total system energy associated with each particular exchange. The probabilities are summed, normalized by this sum and sorted and a random number, R , between 0 and 1, is generated to determine which 1NN exchange is accepted, with the criteria that $P_{i-1} < R \leq P_i$. The solute atoms are randomly chosen (both sub-lattices) to make exchanges until all of the solutes have been exchanged, thereby completing one Monte Carlo step (MCS). Exchanges between like solutes are permitted to ensure every atom has moved at least once and to avoid forced dissolution of clustering atoms. Exchanges between sub-lattices are prohibited. However, both sub-lattices are considered when calculating ΔE .

The system evolves in a sequence of steps towards the lowest free energy, G :

$$G = E - TS_{\text{config}} \quad (2)$$

Where the configurational entropy, S_{config} , is simulated by the Boltzmann weighting. The LMC simulations are not intended to provide a precise description of the details of NC evolution. Instead, they provide insight about the chemical structure of the NCs that can not be determined from standard thermodynamic models. An attempt is made to compare the simulations with experimental sizes and number densities from SANS and compositions from APT.

Parameterization of the Model

The most challenging and important aspect of the modeling effort is the requirement of accurate descriptions of the atomic interactions. As embedded atom method (EAM) potentials for the constituents of this alloy are generally unavailable, pair bond potentials are used (ε_{ii} , ε_{ij} , ε_{jj}). These potentials are derived from thermodynamic data approximated by regular solution theory. The authors acknowledge that this is only a first order approximation and that at least second NN interactions are important to describe interface energies and to accurately treat diffusion in metallic systems. Additionally, as this model relies on a rigid lattice, strain energies are not directly accounted for. Yet, this simplified description can accurately reproduce the alloy thermodynamics and provide atomic level insight into the structure and composition of the precipitates.

The bond energies between like atoms, ε_{ii} , were determined from the cohesive energies, E_{coh} , for the bcc phase of the pure elements as:

$$\varepsilon_{ii} = \frac{2E_{\text{coh}}}{z} \quad (3)$$

where z is the coordination number ($z = 8$ for the BCC structure). As iron is the solvent, this is straightforward and E_{coh} can directly be obtained from the literature [5]. However, yttrium forms a hexagonal close-packed (HCP) phase and it was necessary to perform electronic structure calculations of the cohesive energy, based on local density approximations (LDA) for ε_{YY} with a lattice constant equal to

that of BCC Fe shown in Fig. 1. LDA calculations were also performed for $\varepsilon_{\text{TiTi}}$ and are also shown in Fig. 1.

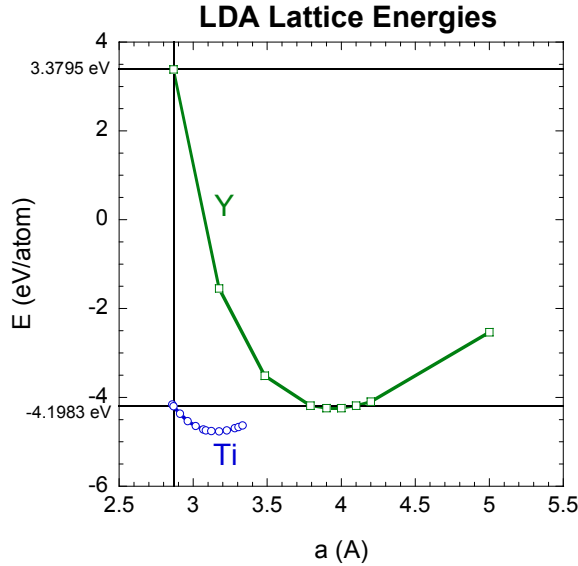


Fig. 1. LDA calculation results for BCC Y and Ti.

The bond energies between different atoms, ε_{ij} , were derived from empirical excess free energies of mixing, ${}^E\Delta G_{ij}$, which include both the excess entropy and enthalpy of solution where:

$$\omega_{ij} = \frac{{}^E\Delta G_{ij}}{z} \quad (4)$$

and

$$\omega_{ij} = \varepsilon_{ij} - (\varepsilon_{ii} + \varepsilon_{jj})/2 \quad (5)$$

Here, ω_{ij} is the interaction parameter and z is the coordination number (8 in BCC). The alloy constituents tend to order if $\omega_{ij}<0$ and phase separate if $\omega_{ij}>0$. Starting estimates for ${}^E\Delta G_{ij}$ were obtained from CALPHAD data, which are used to reproduce and predict phase diagrams [6]. Since the ${}^E\Delta G_{ij}$ represent specific temperatures and compositions, initial values were used from APT information on local chemistries together with nominal alloy composition.

Yttrium is known to be relatively insoluble in BCC iron. Thermodynamic studies have been performed in liquid iron [7] and for the compound phases [8,9]. Therefore, due to the lack of information for the conditions required, the interaction coefficient was obtained from the estimated solubility of Y in Fe using:

$$z\omega_{FeY} = \frac{1}{(1-2X_Y)} kT \ln \frac{1-X_Y}{X_Y} \quad (6)$$

where X_Y is the solubility limit of yttrium in iron at T [9]. Yttrium and titanium are similarly immiscible and there is little thermodynamic information on this system, so the interaction coefficients are again estimated using Equation 6 directly from the phase diagram [10].

Titanium, on the other hand, is reasonably soluble in iron and there have recently been several sets of results published for Ti in BCC Fe [11,12]. Titanium has a negative interaction parameter which indicates a tendency to order in iron [13]. This short range ordering parameter, SRO, can be determined as [14]:

$$SRO = \frac{P_{AB} - P_{AB}(\text{random})}{P_{AB}(\text{max}) - P_{AB}(\text{random})} \quad (7)$$

where P_{AB} is the number of A-B bonds, $P_{AB}(\text{max})$ is the maximum number of A-B bonds possible, and $P_{AB}(\text{random})$ is:

$$P_{AB}(\text{random}) = \frac{zN_A N_B}{(N_A + N_B)} \quad (8)$$

where z is the coordination number and N_A and N_B are the number of A and B atoms in the simulation, respectively.

For the oxygen component, which resides on a separate sub-lattice (octahedral interstitial sites) from the other elements, simple pair interaction parameters are deemed inadequate. In this case, up to 5th NN interactions are included for ϵ_{OO} . This corresponds in distance to about the second NN interactions on the BCC sub-lattice. Unfortunately, to our knowledge, there have been no ab-initio calculations performed for oxygen in iron. However, octahedral nitrogen calculations in iron have been performed by Domain [15]. The reported data can be fit with a Lennard-Jones potential [16] using exponents of 8 and 4 as:

$$\epsilon_{OO}^{iNN} = -\epsilon_{OO}^{iNN} \left[\left(\frac{r_{OO}^{1NN}}{r_{OO}^{iNN}} \right)^8 - 2 \left(\frac{r_{OO}^{1NN}}{r_{OO}^{iNN}} \right)^4 \right] \quad (9)$$

where r_{OO}^{iNN} is the distance between atoms. This data closely duplicates the O₂ bond strength ($1/2E_{O_2} = -2.58$ eV) at the equilibrium O₂ distance ($r_{O_2} = 0.1207$ nm) [17] as shown in Fig. 2.

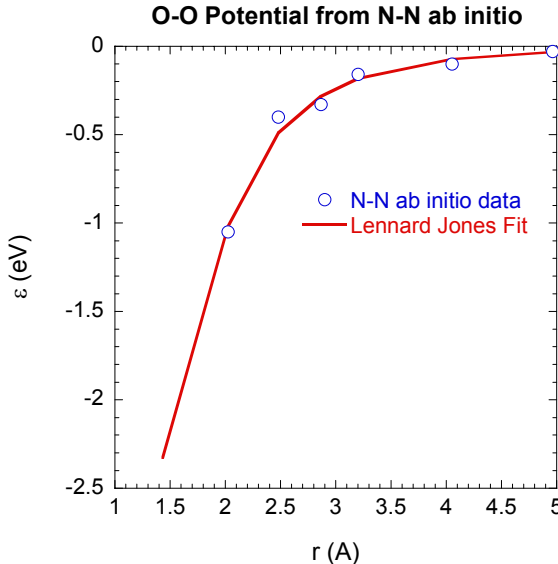


Fig. 2. Lennard-Jones fit to ab-initio calculations of interstitial N in Fe.

The interaction coefficient of Fe and O, ε_{FeO} , was estimated from CALPHAD data [18,19]. However, 2nd NN interactions (to the BCC atom) are now included between the two sublattices. As there is no competition between the two different sublattices of a lattice site, the ε_{ii} and ε_{jj} terms in Equation 5 are omitted and $\omega_{ij} = \varepsilon_{ij}$. To convert the interaction parameter ω_{ij} to first and second neighbor values, the Lennard-Jones potential from Equation 6 is used. The relative proportions of the interaction parameter are assumed to be distributed between the first and second NN as:

$$\Omega_{iO} = 6\varepsilon_{iO}^{1NN} + 12\varepsilon_{iO}^{2NN} \quad (10)$$

There are 6 first NN and 12 second NN bonds. Equations 6 and 7 can then be solved simultaneously to determine the 1st and 2nd NN interactions.

For both yttrium and titanium, the interaction coefficients with oxygen in iron can be determined from the excess energy of formation of Y_2O_3 and Ti_2O_3 in iron where:

$$^E\Delta G = \Omega_{iO} X_i X_O \quad (11)$$

where X_i and X_O are the relative molar fractions of component i (Y and Ti) and oxygen in iron. The activity of oxygen is estimated using Sievert's Law. The excess energy of formation in iron of Y_2O_3 is -17.70 eV and for Ti_2O_3 is -7.96 eV. The ε_{ij} , ε_{ij} and ω_{ij} are shown in Table 1.

Results

Verification of the Parameterization

Verification of the system interaction parameters was performed using simulation cells of 5,488 BCC lattice sites (21,952 total sites) equivalent to a cell of 14x14x14 unit BCC Fe cells (4.01x4.01x4.01 nm³). The simulations were each performed for 5M MCS, enough to bring the systems to their lowest energy states.

Based on the Fe-Y interaction parameter, ω_{FeY} , the yttrium is anticipated to phase separate in iron. With increasing temperature, some Y will become soluble in the iron due to the limited solubility as well as the Gibbs-Thomson effect. The results for the system energy for Fe-1.0Y as a function of the MCS are shown in Fig. 3. The solubility can be expressed as $X_Y = 4 \times 10^{-31} T^{8.81}$.

Table 1. Interaction parameters in Fe-Ti-Y-O system

$\varepsilon_{\text{FeFe}}$	-1.07 eV	$E_{\text{coh}}(\text{Fe})$	4.28 eV
ε_{YY}	0.84 eV	$E_{\text{coh}}(\text{Y})$	4.37 eV
$\varepsilon_{\text{TiTi}}$	-1.05 eV	$E_{\text{coh}}(\text{Ti})$	4.85 eV
ε_{FeY}	0.02 eV	ω_{FeY}	0.13 eV
$\varepsilon_{\text{FeTi}}$	-1.13 eV	ω_{FeTi}	-0.52 eV
ε_{YTi}	-0.03 eV	ω_{YTi}	0.07 eV
$\varepsilon_{\text{OO}}^{1\text{NN}}$	-2.33 eV		
$\varepsilon_{\text{OO}}^{2\text{NN}}$	-1.02 eV		
$\varepsilon_{\text{OO}}^{3\text{NN}}$	-0.49 eV	$E_{\text{coh}}(\text{O})$	2.60 eV
$\varepsilon_{\text{OO}}^{4\text{NN}}$	-0.28 eV		
$\varepsilon_{\text{OO}}^{5\text{NN}}$	-0.18 eV		
$\varepsilon_{\text{FeO}}^{1\text{NN}}$	-0.42 eV	ω_{FeO}	-0.59 eV
$\varepsilon_{\text{FeO}}^{2\text{NN}}$	-0.18 eV		
$\varepsilon_{\text{YO}}^{1\text{NN}}$	-8.89 eV	ω_{YO}	-12.50 eV
$\varepsilon_{\text{YO}}^{2\text{NN}}$	-3.89 eV		
$\varepsilon_{\text{TiO}}^{1\text{NN}}$	-2.83 eV	ω_{TiO}	-3.98 eV
$\varepsilon_{\text{TiO}}^{2\text{NN}}$	-1.24 eV		

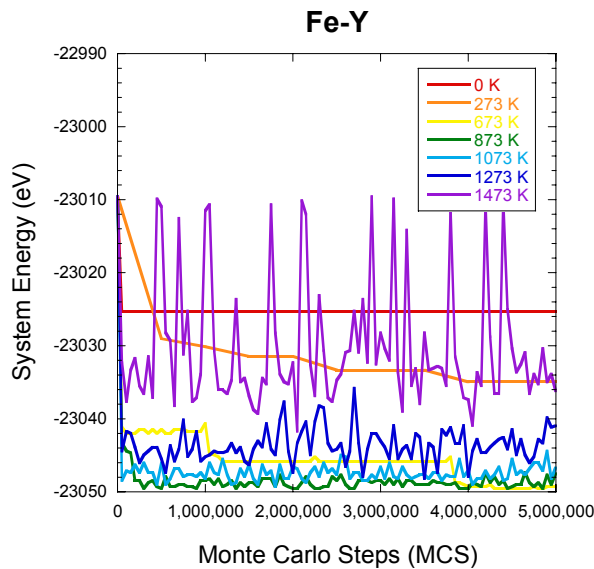


Fig. 3. System energy evolution for Fe-1.0Y from 273K-1473K.

Titanium will order in iron, as shown in Fig. 4. At 273K, nearly perfect ordering is achieved. However, the configurational entropy term, TS_{config} , begins to play a more significant role with increasing temperature and the SRO drives toward a random solution.

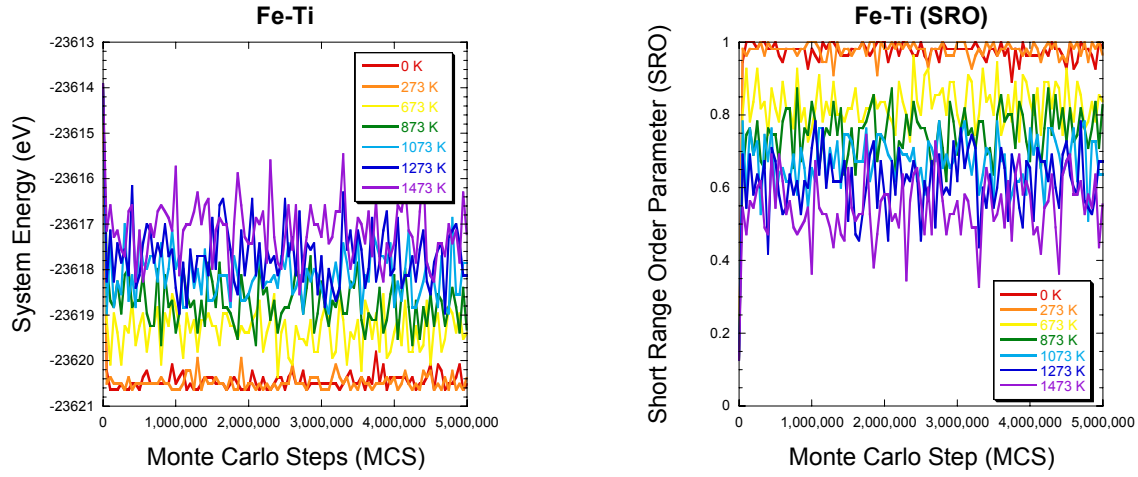


Fig. 4. System energy evolution and SRO for Fe-5.0Ti from 273K-1473K.

The results for oxygen in iron is shown in Fig. 5. The interaction parameter indicates that oxygen should order in Fe and, in fact, at these high concentrations does. Interestingly, the configurational entropy term does not appear to play a significant role as the system energy reaches a similar steady state value for all temperatures.

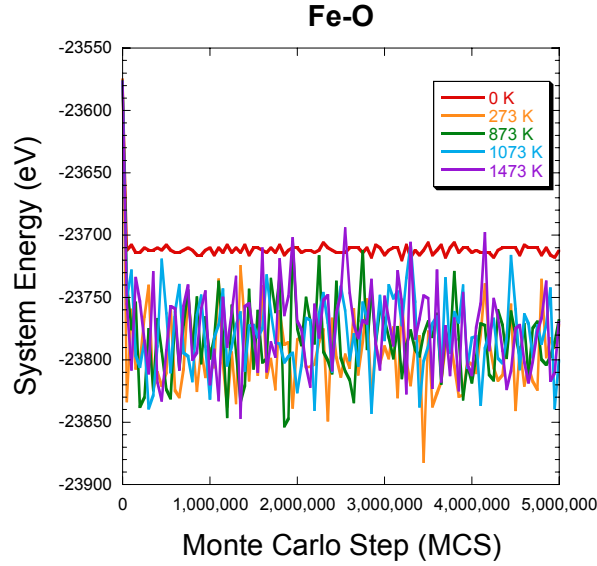


Fig. 5. Oxygen.

In the ternary system, Fe-Y-O, the Y and O cluster as shown in the snapshot in Fig. 6, as anticipated by the interaction parameters.

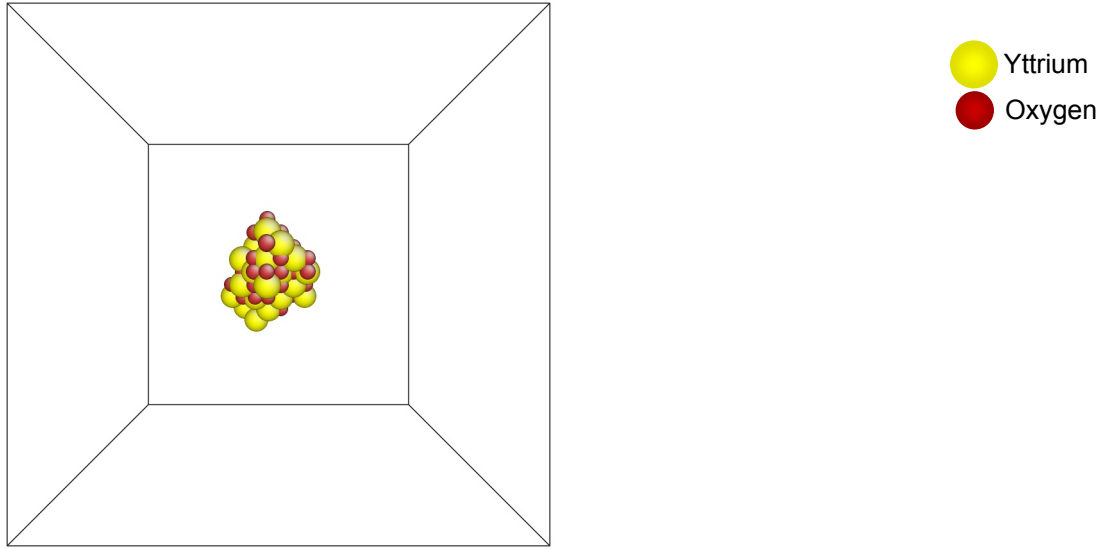


Fig. 6. Fe-Y-O.

For the Fe-Ti-O system, the Ti and O also cluster as shown in the snapshot in Fig. 7.

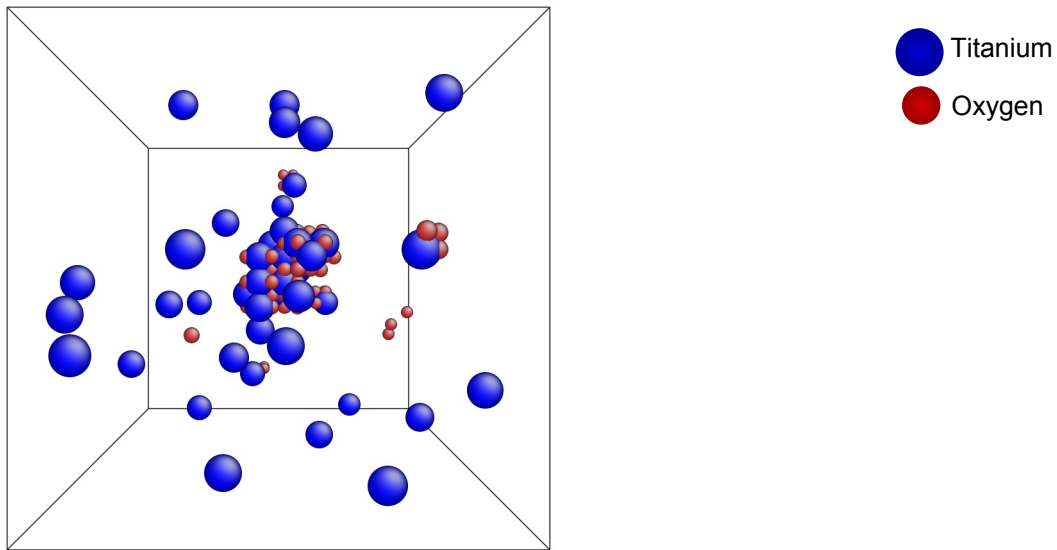


Fig. 7. Fe-Ti-O.

Finally, in the Fe-Ti-Y system, the Y clusters, with little to no incorporation of Ti, as shown in the snapshot in Fig. 8.

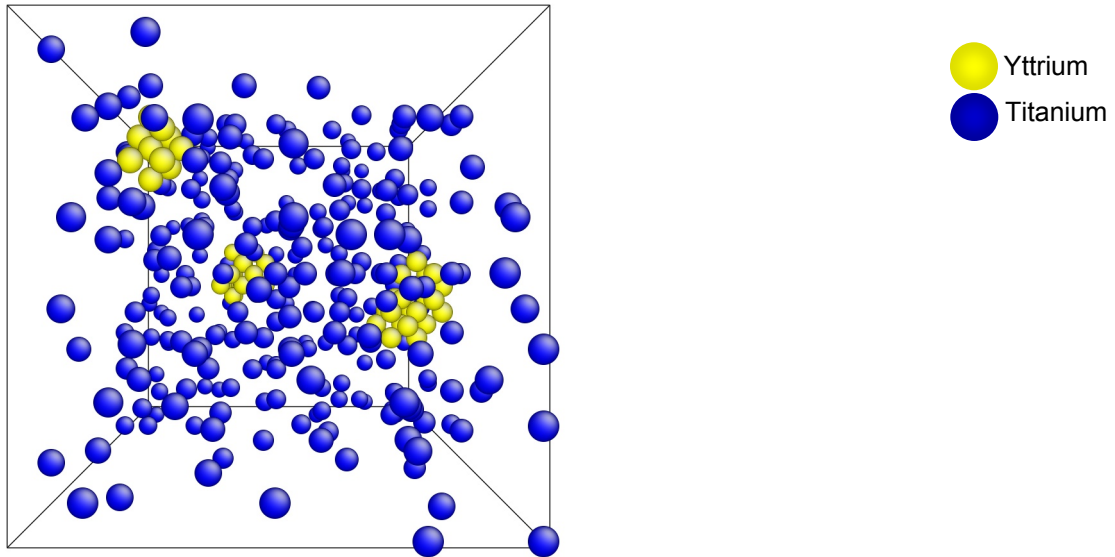


Fig. 8. Fe-Ti-Y.

Full Simulation

The initial results of a full system simulation are shown in Fig. 9. This simulation was performed using a 42x42x42 unit cell which contains 148,176 BCC lattice sites (592,794 total sites). This is equivalent to $12.04 \times 12.04 \times 12.04 \text{ nm}^3$. The single final precipitate in this cell is equivalent to a precipitate number density of $5.7 \times 10^{23} \text{ m}^{-3}$.

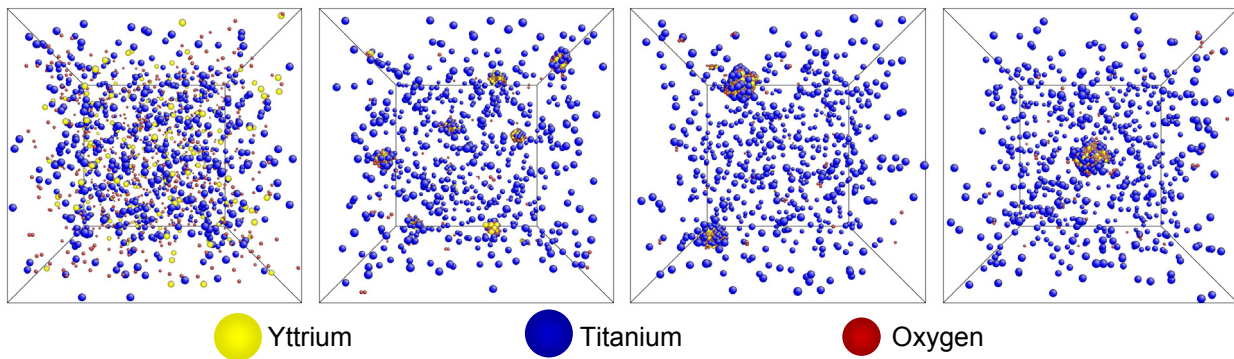


Fig. 9. Simulation of Fe-0.46%Ti-0.12%Y-0.43%O at 673K for 3.5M MCS.

An enlarged view of the precipitate structure and composition is shown in Fig. 10. The Ti is segregated to the outer surface of the 0.90 nm radius precipitate and the composition is about 23%Y-9Ti-68O. Regardless of the temperature or size, Ti is observed to segregate to the interface, which is consistent with atom probe measurements reported by Miller for NC in MA957 [20].

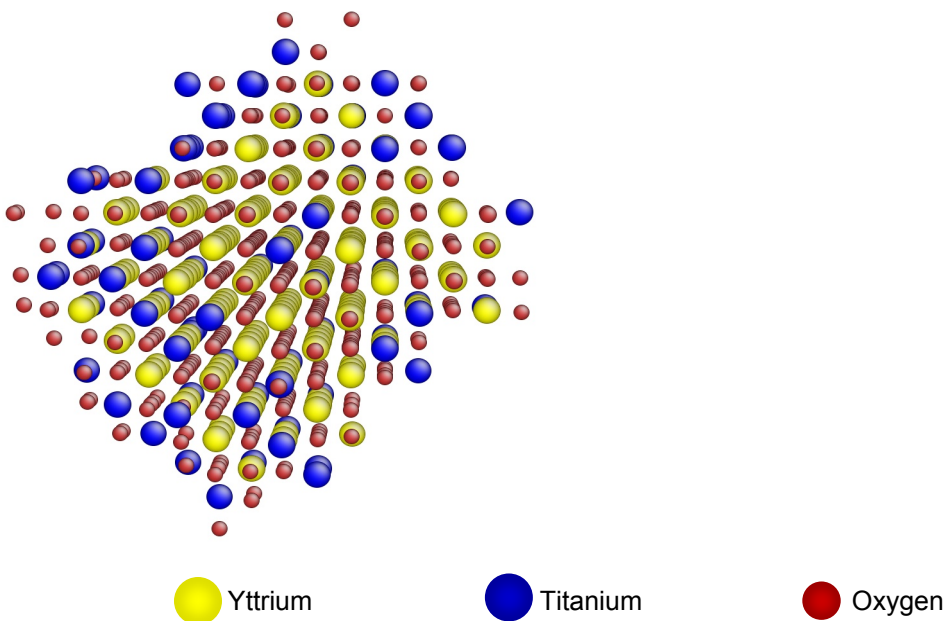


Fig. 10. NC composition for Fe-0.46Ti-0.12Y-0.43O simulation.

Future Work

Future work will focus on the following items:

1. Larger simulation cells (2M BCC atoms) for improved stochastic information.
2. Study the effects of temperature on NC composition.
3. Study the effects of excess oxygen on NC composition.
4. Study the effects of lattice strain energy.
5. Evaluate the formation energy of the NCs.
6. Evaluate the dissolution energy/binding energy.
7. Thorough comparison of the simulation results with SANS and APT data.

Acknowledgements

The authors would like to thank Hyon-Jee Lee for graciously calculating the LDA cohesive energies for Y and Ti on a BCC Fe lattice. This work has been supported by the Office of Fusion Energy Sciences, U.S. Department of Energy, under Grant DE-FG02-04ER54750.

References

- 1 M. J. Alinger, G. R. Odette, and D. T. Hoelzer, *J. Nucl. Mater.* 329–333 (2004) 382.
- 2 S. Ukai and M. Fujiwara, *J. Nucl. Mater.* 307–311 (2002) 749.
- 3 H. Kishimoto, M. J. Alinger, G. R. Odette, and T. Yamamoto, *J. Nucl. Mater.* 329–333 (2004) 369.
- 4 M. J. Alinger, *On the Formation and Stability of Nanometer Scale Precipitates in Ferritic Alloys During Processing and High Temperature Service*, dissertation submitted in partial fulfillment of Ph.D. degree in Materials from the University of California, Santa Barbara (2004).
- 5 C. Kittel, *Introduction to Solid State Physics*, John Wiley & Sons, Inc., New York (1996).
- 6 U. R. Kattner, *JOM* 49 (1997) 14.
- 7 D. U. Ting and W. Longmei, *J. Less-Common Metals* 110 (1985) 179.

- 8 R. Coehoorn, Phys. Rev. B 39 (1989) 13072.
- 9 P. R. Subramanian and J. F. Smith, Calphad 8 (1984) 295.
- 10 J. L. Murray, Binary Alloy Phase Diagrams, ASM, Metals Park, Ohio (1986).
- 11 K. C. Hari Kumar, P. Wollants, and L. Delaey, Calphad 18 (1994) 223.
- 12 S. Jonsson, Metall. Mater. Trans. B 29 (1998) 361.
- 13 J. Cieslak and S. M. Dubiel, J. Alloy. Compd. 387 (2005) 36.
- 14 D. A. Porter and K. E. Easterling, Phase Transformations in Metals and Alloys, Nelson Thornes Ltd., Padstow (2001).
- 15 C. Domain, C. S. Becquart, and J. Foct, Phys. Rev. B 69 (2004).
- 16 R. Furth, Proceedings of the Royal Society of London, Series A, Math. Phys. Sci. 183 (1944) 87.
- 17 CRC, Handbook of Chemistry and Physics, 51st Ed., R. C. Weast (ed.), CRC Press, Cleveland, Ohio (1970) F-57.
- 18 M. Kowalski and P. J. Spencer, Calphad 19 (1995) 229.
- 19 P. J. Spencer and O. Kubaschewski, Calphad 2 (1978) 147.
- 20 M. K. Miller, D. T. Hoelzer, E. A. Kenik, and K. F. Russell, Intermetallics 13 (2005) 387.